2019

Highly Selective Fluorimetric Turn-Off Detection of Copper (II) by Two Different Mechanisms in Calix[4]arene-Based Chemosensors and Chemodosimeters

Justine O'Sullivan
National University of Ireland, Maynooth

John Colleran
Technological University Dublin, john.colleran@tudublin.ie

Brendan Twamley
Trinity College Dublin, Ireland

Frances Heaney
National University of Ireland, Maynooth, frances.heaney@mu.ie

Follow this and additional works at: https://arrow.tudublin.ie/aegart

Part of the Other Chemistry Commons

Recommended Citation

Technological University Dublin

Highly Selective Fluorimetric Turn-Off Detection of Copper (II) by Two Different Mechanisms in Calix[4]arene-Based Chemosensors and Chemodosimeters

Justine O'Sullivan,[a] John Colleran,[b] Brendan Twamley,[c] and Frances Heaney*[a]

Isoxazolo-pyrene tethered calix[4]arenes selectively detect copper(II) ions without interference from related perchlorate ions. The fluorescence emission of the probes, synthesised by nitrile oxide alkyne cycloaddition, and characterised by spectroscopic and crystallographic data, is rapidly reduced by Cu(II) ions. Detection limits are in the micromolar or sub-micromolar range (0.3–3.6 μM) based on a 1:1 sensor:analyte interaction. Voltammetric behaviour and ^1H NMR data provide new insights into the sensing mechanism which is dependent on the calixarene substitution pattern. When the calixarene lower rim is fully substituted, Cu(II) detection occurs through a traditional chelation mechanism. In contrast, for calixarenes 1,3-disubstituted on the lower rim, detection takes place through a chemodosimetric redox reaction. The isolation of a calix[4] diquinone from the reaction with excess $Cu(ClO_4)_2$ provides confirmation that the sensor–analyte interaction culminates in irreversible sensor oxidation.

Introduction

The design of new materials to remove or to monitor the levels of potentially toxic metals ions from water samples is an important area of contemporary research.[1] The juxtaposition of copper ions as biologically necessary and environmentally toxic means that selective and sensitive monitoring of copper ions is important for human health and industrial activity.[2] In this context Cu(II) selective chemosensors and chemodosimeters are highly prized and a variety of detecting platforms have been developed including gold and carbon nanoparticle probes,[2b,3] mesoporous materials[1i,k, 4] and enzymatic systems.[5] Whilst transition metal ion sensors generally rely on metal ion binding, chemodosimetric Cu(II) detection is receiving increasing attention. A range of chemistries including irreversible aryl ether cleavage,[6] imine hydrolysis,[7] redox chemistry inducing phenothiazine oxidation,[8] dihydropyrazine oxidation,[9] ring opening of rhodamine B derivatives[10] and specific click ligation[11] have been used to sense copper cations. Copper detection is amenable to a diverse range of assays including electrochemical, chromogenic and fluorogenic.[12]

We recently reported the fluorogenic recognition of Cu(II) ions by a calix[4]arene framed isoxazole-pyrene sensor, **S1**.[13] To understand the sensing mechanism a series of molecules related to **S1** but each differing in one key structural feature have been studied: **S2** incorporates a propyl spacer between the pyrene and isoxazole moieties whilst a two carbon linker separates the calix[4]arene lower rim and the heterocycle in **S3**, finally, the lower rim phenolic OH groups are fully substituted in **S4**, Figure 1. In a series of elegant papers Chung and co-workers report calixarene framed Cu(II) sensors related to **S1-4** with β-amino α,β-unsaturated ketone,[14] amide[15] isoxazole[14,16] or 1,2,4-oxadiazole[17] as metal ion binding motifs, paired with naphthyl, anthryl or chloroanthryl reporting units. Chung's data suggests a Cu(II) detection mechanism sensitive to the calixarene substitution pattern, specifically, when there are unprotected phenolic groups, and where the large rim is unsubstituted a metal-ligand charge transfer band in the UV spectrum implicates a Cu(I)-phenoxy radical complex.[14–15] However, no such band presents with upper rim substituted calixarene sensors.[16] The current work is focused towards understanding the relationship between the structure of the calixarene framed sensors **S1-S4** and their mechanism of metal ion detection. It reports the synthesis, structure characterisation and sensing capacity of the new sensors and presents a hypothesis, formulated on the basis of cyclic voltammetry and spectroscopic studies, to account for their unique interactions with Cu(II) over related transition metal ions.

[a] Dr. J. O'Sullivan, Prof. F. Heaney
Department of Chemistry
Maynooth University,
Maynooth, Co. Kildare W23 F2H6 (Ireland)
E-mail: Frances.heaney@mu.ie
[b] Dr. J. Colleran
School of Chemical & Pharmaceutical Sciences,
and Applied Electrochemistry Group
Focas Institute, Camden Row
Technical University Dublin
Kevin Street, Dublin 8 D08 NF82 (Ireland)
[c] Dr. B. Twamley
School of Chemistry,
Trinity College Dublin, University of Dublin,
Dublin 2 (Ireland)
Supporting information for this article is available on the WWW under
https://doi.org/10.1002/cplu.201900448
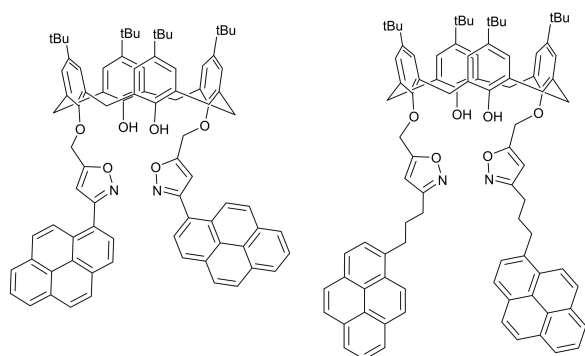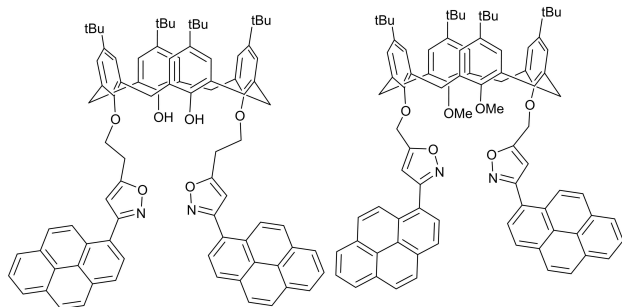
Figure 1. Structures of the isoxazolo-pyrene tethered calix[4]arene sensing molecules **S1-S4**.

Results and Discussion

Synthesis and Characterisation of S2-S4

The heterocycle and the fluorescent pyrene units were installed at the lower rim of a *t*Bu-capped calix[4]arene by catalyst free nitrile oxide alkyne cycloaddition (NOAC) chemistry,[18] Scheme 1. To access **S2** and **S3** the required distal alkylated **1** and **2** were prepared by reported methods involving K_2CO_3 induced alkylation of 4-*tert*-butylcalix[4]arene with propargyl bromide or 4-bromo-1-butyne respectively.[19]

The novel 1-pyrenebutanaldoxime, **3**, was required to access **S2** whilst known 1-pyrenecarbaldoxime[20] was needed to prepare **S1**, **S3** and **S4**. The aldehyde precursor to the latter was commercially available whilst 1-pyrenebutanal was prepared
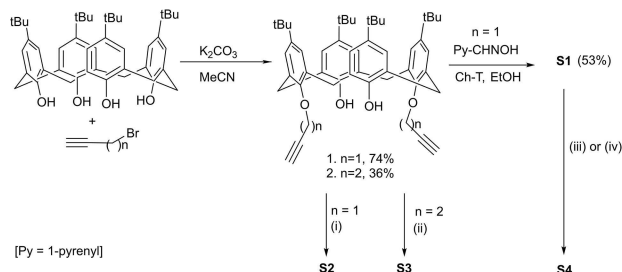
Scheme 1. Synthesis of sensors **S1-S4** by catalyst-free nitrile oxide alkyne cycloaddition chemistry. (i) Py(CH$_2$)$_3$-CHNOH, NCS, DCM, rt, 1 h, 49%; (ii) NEt$_3$, Py-CHNOH, Ch–T, EtOH, 24 h, reflux, 49%; (iii) NaH, MeI, DMF, 24 h, rt, 62%; (iv) Cs$_2$CO$_3$, MeI, acetone, 17 h, rt, 71%.
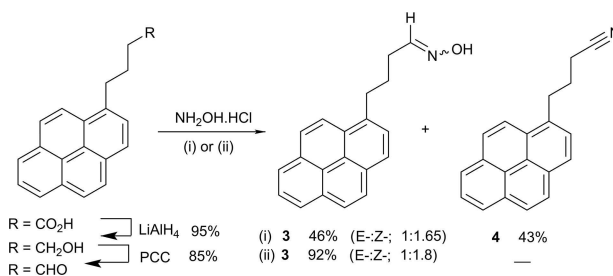
Scheme 2. Synthesis of 1-pyrenebutanaldoxime **3**.

from the acid following lithal reduction to the known alcohol[21] (95%) and pyridinium chlorochromate (PCC) oxidation[22] (85%), Scheme 2. Oximation was sensitive to the experimental conditions and dehydration to the nitrile **4** was a complication of the initial reaction executed in a scientific microwave (125 °C, 1 hour, P$_{max}$ 300 W) with pyridine as base. Gratifyingly, a NaOAc induced reaction in refluxing aq. MeOH furnished **3** in 92% yield, as a 1:1.8 mixture of E- and Z-isomers.

The preferred approach to nitrile oxide formation from aliphatic oximes involves *in situ* halogenation and dehydrohalogenation,[23] thus, **3** was treated with *N*-chlorosuccinimide (NCS) in DCM at room temperature (rt) prior to NEt$_3$ induced dehydrohalogenation. **S2** was isolated as an off-white solid in 49% yield following trapping of the putative dipole by the bis-propargylated **1**. To access **S3**, with a two-carbon spacer between the isoxazole ring and the calixarene lower rim, the butynylcalix[4]arene **2** was used to trap the putative dipole formed from reaction of 1-pyrenecarbaldoxime with chloramine-T (Ch—T). The oxime was used in excess (2 eq. per alkyne functional group) and to minimize nitrile oxide side reactions the Ch—T was added in three portions. After purification **S3** was obtained as a crystalline solid (49%). Synthesis of the fully substituted **S4** was achieved by methylation of **S1**, mediated either by NaH[13] in dimethyl formamide (DMF) at rt (62%), or, more attractively with Cs$_2$CO$_3$ in refluxing acetone (71%), Scheme 1.

High resolution mass spectrometry and NMR spectroscopic data support the structures of **S2-S4**. The isoxazole rings are 3,5-disubstituted and the C-4 carbon atoms resonate at ~103–105 ppm (125 MHz, CDCl$_3$). The propyl spacer reduces the impact of the pyrene moiety on the isoxazole-H of **S2** causing an ~0.6 ppm upfield shift with respect to the corresponding signals for **S1** and **S3** where π-electron delocalisation between the rings is possible. The relationship between the isoxazole and pyrene rings also influences the calix-O-CH$_2$-protons which for **S2** and **S3** appear upfield, (~0.3 and ~1.4 ppm respectively), of the equivalent protons of **S1**. The NMR data points to solution state cone conformations; the diastereotopic methylene protons of the calix[4]arene framework resonate as sharp AB doublets with ~13.0 Hz coupling constants between the shielded *endo*- and the deshielded *exo*-protons.[24] The downfield phenolic proton resonances, >6.5 ppm, also support lower rim H-bonding and calixarene cone conformations.

Broad signals in the rt 1H NMR spectrum of **S4** (300 MHz, CDCl$_3$) point to conformational conversion on the NMR time-

scale consequent of the lack of lower rim H-bonding opportunities, and the potential for intra-annular movement of the sterically undemanding methoxy group. In an effort to improve quality, spectra were recorded over a range of temperatures. Resolution continued to deteriorate up to 45 °C, Figure S27 (see the Supporting Information), however, a gradual improvement was observed below rt. Spectra recorded at −30 °C (500 MHz, CDCl$_3$) support the presentation of **S4** as a mixture of cone and paco-OMe conformers. Key resonances are summarised in Table 1.

Table 1. Key NMR spectroscopic data in support of the presentation of **S4** as a mixture of cone and paco-OMe conformers (500 MHz, −30 °C, CDCl$_3$).

Conformer	δ$_H$, [multiplicity, J]	Relative integral[a]	δ$_C$
Upper rim *t*Bu			
paco-OMe[b]	1.34, 1.11, 1.07 (3×s)	1:1:2	
cone	1.31, 0.87 (2×s)	1:1	
Calix[4]arene Ar-H			
paco-OMe	7.30 (s); 7.14 (s)[c] 7.00 (d, 2 Hz) & 6.60 (d, 2 Hz)	1:1:1:1	
cone	7.14 (s)[c]; 6.57 (s)	1:1	
Lower rim methylene			
cone	4.43 (d, 12.7 Hz) & 3.27 (d,12.7 Hz)	1:1	~31
paco-OMe	4.23 (d,12.9 Hz) & 3.20 (d,13.2 Hz) & 3.86 (d, 14.1 Hz) & 3.79 (d,14.1 Hz)	1:1 1:1	~31, 37.8
OCH$_2$-Isoxazole			
cone	5.11, s		67.3
Paco-OMe	4.88 (d, 12.3 Hz) & 5.12 (d, 12.3 Hz)	1:1	65.7
Isoxazole			
cone	6.90, s		105.2
paco-OMe	6.82, s		105.7

[a] Relative integrals of a series of signals for a given conformer; [b] Paco—OMe denotes the structure where the Ar—OCH$_3$ ring points anti to the other rings of the calix[4]arene framework of **S4**; [c] coincident signals.

There is an established relationship between calix[4]arene conformation and the chemical shift of the bridging methylene carbon atoms; when adjacent aryl rings are syn related a resonance is expected at ~31 ppm, when they are in an anti-relationship the signal appears ~37 ppm.[25] The DEPT-135 spectrum of **S4** (−30 °C, CDCl$_3$) displays three resonances in this window consistent with both paco-OMe and cone conformers. A ^{1}H^{1}H COSY spectrum revealed three pairs of lower rim diastereotopic methylene protons represented by six doublets. The resonance position, the chemical shift difference, and the size of the coupling constant between the mutually paired signals also characterise the sample as a mix of conformers.[26] One pair with well-separated chemical shifts, 4.43 & 3.27 (J 12.7 Hz) arise from the cone conformer. Two further pairs, one well-separated [4.23 & 3.20 (J 13.2 Hz)] and another with very similar chemical shifts [3.86 & 3.79 (J = 14.1 Hz)] originate from the paco-OMe conformer.[26] Five distinct signals in the *t*Bu region represent paco [1.34, 1.11 & 1.07 ppm; 1:1:2 ratio] and cone conformers [1.31 & 0.87 ppm; 1:1 ratio]. The upper rim

calix-ArH resonate in the range 7.30–6.57. The non-equivalent protons of the rings adjacent to the inverted ring of the paco conformer appear as two doublet signals, 6.60 and 7.00 ppm (^{4}J ~ 2 Hz). A singlet at 6.57 ppm is attributed to the cone conformer. The second ArH resonance of this conformer, coincident with a signal of the paco conformer, appeared at 7.14 ppm. The remaining paco-ArH resonated at 7.30 ppm. The resonances of the pyrene nuclei are not unambiguously assigned due to severe overlap. Three singlet resonances represent the methoxy groups of **S4**; the equivalent protons of the cone conformer appear at 4.00 ppm. Signals at 3.37 and 3.34 ppm, baseline resolved and in a 1:1 ratio, represent the non-equivalent methoxy protons of the paco conformer. Cross peaks in the HSQC spectrum at 105.2 & 6.82 ppm, and 105.7 & 6.90 ppm, represent, respectively, the isoxazole C—H of the paco and cone forms of **S4**. The relative integrals of the *t*Bu, ArH and isoxazole-H signals concur with an ~1:2.8 equilibrium population of cone and paco conformers at −30 °C in CDCl$_3$.

Solid-State Structures

We previously reported the structure of **S1** as an acetonitrile solvate,[13] we now report it co-crystallised with DCM, Figure 2. The calix[4]arene is in a slightly asymmetric cone formation stabilised by hydrogen bonds between the lower rim OH groups and the ether oxygen atoms [O1…O15 = 2.696(8); O23…O31 = 2.730(8) Å]. Cone diameters were measured at 8.443(12) & 7.898(1) Å for the upper, and at 3.803(9) & 4.079(8) Å for the lower rim. The isoxazolo-pyrene pendants do not stack, they have free rotation and are twisted in relation to each other; ring plane normal isoxazole pyrene twist angles 39.674(3) & 148.622(3)°. The isoxazole-pyrene torsion angles are similar [140.1(9) and 149.6(9)°]. One DCM molecule is sited chlorine down in the cone cavity. The other is external to the cavity and lies near one of the isoxazole rings. The molecules pack as pairs with interdigitating tail ligands yet there are no

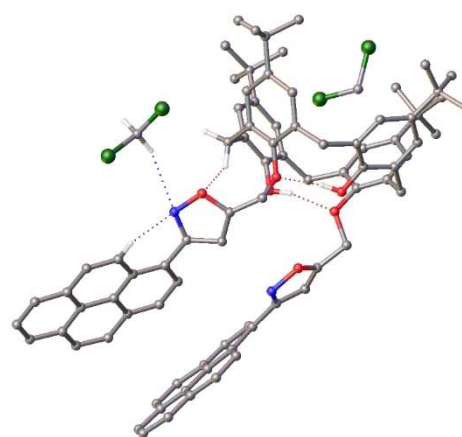
Figure 2. Asymmetric unit of **S1.2DCM** with only hydrogen atoms involved in H-bonding interactions shown. DCM solvent molecules shown within and also without the calix[4]arene cone. Dashed lines indicate OH…O and CH…O and CH…N interactions.
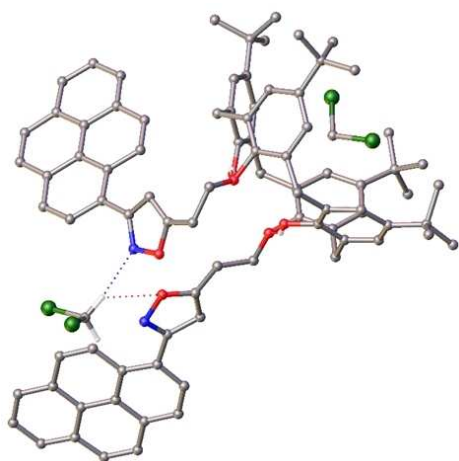
Figure 3. Asymmetric unit of **S3·2DCM** with only hydrogen atoms involved in H-bonding interactions shown. Dashed lines indicate CH…O and CH….N interactions.

Figure 4. Partial packing diagram of **S3** viewed normal to the π–π plane showing intermolecular π-π stacking between neighbouring pyrene units.

significant intermolecular interactions. The pairs form stacks parallel to the b-axis with solvent channels between and terminating each stack, Figure S54.

We were unable to obtain x-ray quality crystals from **S2**. It is likely that the flexible propyl chain between its pyrene and isoxazole moieties was not conducive to regular packing, however, **S3**, like **S1**, co-crystallised with two molecules of DCM, Figure 3. Two of the *t*Bu groups on the upper rim were modelled as disordered over two positions and one DCM within the cavity is also disordered. The lower rim phenolic OH and ether oxygen atoms are involved in intramolecular hydrogen bonding; [O1…O2 = 2.85870(8); O3…O4 = 2.80267(10) Å]. Unlike **S1**, the DCM is CH_2 'down' in the cavity, with both Cl atoms 'up'. The upper rim cone diameter is 7.38213(18) & 9.2420(3) Å and the lower is 3.21620(9) & 4.49412(11) Å showing the **S3** cone as more pinched than **S1** to accommodate DCM CH_2 'down'. The extra carbon in the ether chain leads to more degrees of freedom. The isoxazolo-pyrene torsion angles at −141.658(1) and −153.608(1)° are only slightly more pronounced whilst the ring plane normal isoxazole pyrene twist angles at 42.2990(11)° and 25.3408(8)° differ more significantly from those measured for **S1**. As for **S1** the external DCM, while disordered is involved in weak intermolecular interactions linking the two isoxazole rings together. This engagement brings one isoxazole into an intramolecular interaction distance from the pyrene with a bifurcated interaction of C78…N73, 2.88417(11) Å and a longer weaker intermolecular interaction between C78…Cl3, 3.63537(9) Å. Significantly, the packing of **S3** involves intermolecular π-π stacking between neighbouring pyrene units, Figures 4 and S55. Face-to-face overlap, [plane to plane centroid = 3.37501(8) Å], was evident between one pyrene moiety of each molecule and its symmetry generated neighbour [C53–C66 symmetry code 1-x, 1-y, 1-z]. Attainment of this alignment may be facilitated by coordination of the isoxazole heteroatoms to a solvent molecule, and by the increased flexibility offered by the additional lower rim methylene hinge on **S3**. The second pyrene unit of each discrete **S3**
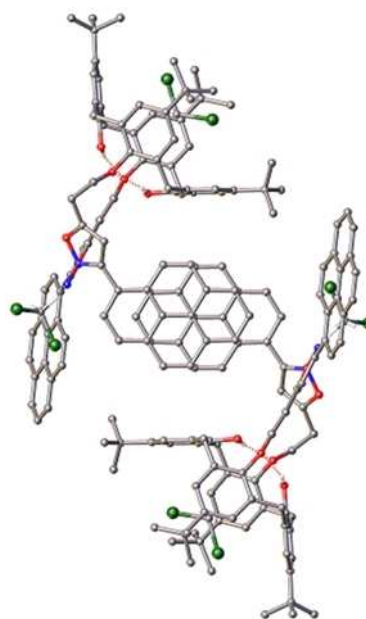
molecule was not involved in either inter- or intramolecular π-π stacking.

S4, with lower rim methoxy substituents crystallised free of solvent, as the paco-OMe conformer, Figure 5. The planes of two of the phenyl rings of the calix[4]arene framework are almost parallel [C1 ring, C9 ring plane normal angle 3.53(13)°] and the flipped ring, is almost perpendicular to these two rings [C1 ring to C15 ring plane normal 93.15(12), C9 ring to C15 ring plane normal angle 91.41(13)°]. The remaining ring is canted outwards, the ring plane normal C3 to C15 angle is 118.57(13)°. The diameter of the lower rim is 5.480(4) Å (O2…O4). As a consequence of the subtended *t*Bu group from the partial cone conformation the isoxazole rings are pushed out and the neighbouring pyrene groups cup this aliphatic region. The
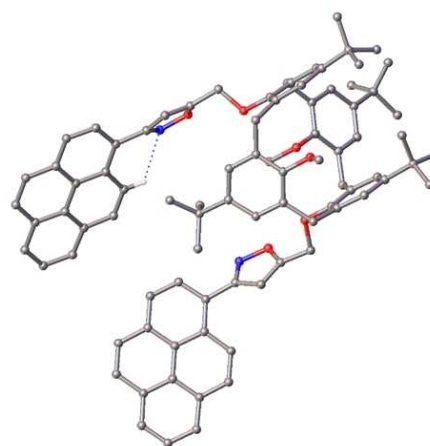

Figure 5. Asymmetric unit of **S4** with only hydrogen atoms involved in H-bonding interactions shown. Dashed line indicate CH….N interactions.

pyrenes 'face' the same direction with torsion angles $-139.0(4)$ and $-46.4(4)°$ [N50-C51-C53-C66 and N72-C73-C75-C88 respectively]. Isoxazole to pyrene plane normal to plane normal are $140.91(11)$ and $50.27(12)°$. The packing of **S4** is more regular than either **S1** or **S3** and the paco-arrangement allows the molecules to efficiently pack in a head (*t*Bu)-to-tail (pyrene) arrangement with no significant intra or intermolecular interactions, Figure S56. Comparative structural features of **S1**.2DCM, **S3**.2DCM and **S4** are compiled in Table S2: CCDC 1940024–1940026 contains the supplementary crystallographic data for this paper. These data can be obtained free of charge from The Cambridge Crystallographic Data Centre.

Photophysical Properties

In common with pyrene[27] and its aliphatically substituted derivatives[28] three absorption bands centred around 240, 280 and 348 nm are present in the UV spectra of **S2-S4** (MeCN, 6 μM), Figure 6a. The bands for **S3** and **S4** with directly
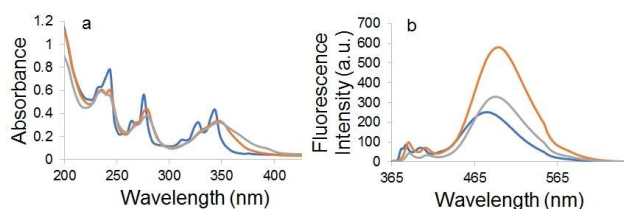
Figure 6. (a) Absorption and (b) fluorescence emission spectra (λ_{ex} 348 nm) of **S2** (blue), **S3** (orange) and **S4** (grey), (6 μM, MeCN).

connected pyrene and isoxazole moieties have limited fine structure, however, **S2** displays well-defined vibronic structure. On the basis of this data the fluorescence emission spectra of **S2**–**S4** were acquired with excitation at 348 nm (6 μM, MeCN, λ_{ex} 348). All three compounds showed dual fluorescence with monomer and featureless excimer emission bands, Figure 6b. Plots of fluorescence emission intensity (at λ_{max}) against concentration were linear up to 10 μM in MeCN indicating excimer emission originates from intramolecular interaction of excited state pyrene nuclei. Concentration dependent quenching was observed beyond these levels, Figure S38. The relative intensity of the excimer to monomer emission bands, I_e, defined as $I_e (\%) = I_e/(I_e + I_m)$, where I_e and I_m are the emission intensities at the excimer band and the first monomer signal respectively, spanned 74–91%. It is likely that the flexible propyl chain between the pyrene and isoxazole moieties of **S2** explains both the diminished intensity and the reduced dominance of the excimer band (I_e 74%). The methoxy-substituted **S4** showed a low intensity excimer band with respect to the unsubstituted **S1** (328 vs 737 a.u.), however, equilibration between the cone and paco conformers apparently does not disproportionately influence excimer formation and the I_e (%) values for **S4** (88) and **S1** (91.5) are comparable. An evaluation of the fluorescence profiles of **S1-4** indicates that **S1**'s architecture, involving a

direct linkage between the isoxazole and the pyrene components and incorporating a single methylene linker between the calix[4]arene lower rim and the isoxazole maximizes excimer emission in MeCN.[13]

Metal-Ion Sensing Properties

The spectrofluorometric response of 6 μM MeCN solutions of **S2-S4** to 100 equivalents of the perchlorate salts of mercury, nickel, zinc, cobalt, lead, manganese, calcium, silver and copper was measured one minute following mixing of the sensor and analyte samples in the cuvette. Significant changes were observed only on exposure to Cu(II), Figure 7. For **S2** an
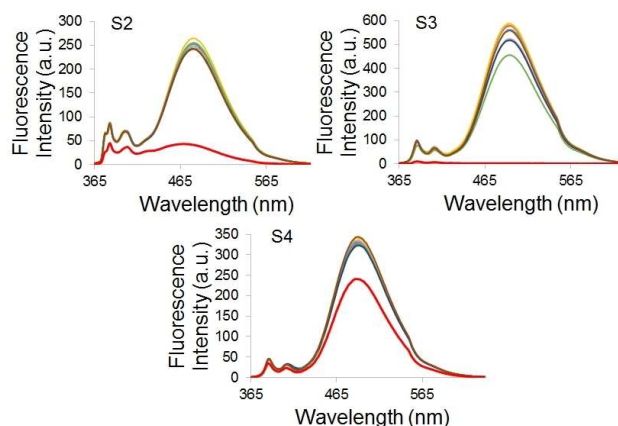
Figure 7. Fluorescence emission spectra of **S2-S4** (6 μM, λ_{ex} 348 nm) in MeCN with 0 (blue) and 100 eqs of $M^{n+}(ClO_4^-)_n$ where $M^{n+} = Ca^{2+}, Pb^{2+}, Mn^{2+}, Zn^{2+}, Hg^{2+}, Ni^{2+}, Co^{2+}$ or Ag^+. The red trace is for each sensor in the presence of $Cu(ClO_4)_2$.

approximate 83% quench, signal broadening and a blue-shift (10 nm) of the λ_{max} of the excimer band was noted. $Hg(ClO_4)_2$ and $Co(ClO_4)_2$ were the only other salts to effect excimer quenching, each at ~4%. **S3** was more sensitive than **S2** to Cu (II) and complete quenching was observed, however, selectivity was challenged and moderate to low quenching was also observed with the perchlorate salts of Hg(II) (~21%), Co(II) (9%) and Pb(II) (7%). **S4**, with the fully substituted lower rim, was least sensitive to $Cu(ClO_4)_2$ with 100 equivalents eliciting only ~27% excimer selectivity was good and $Hg(ClO_4)_2$ was the only other salt to give a detectable response, (~3% quenching).

Competition experiments showed the efficiency of Cu(II) detection was unperturbed by the presence of potential contaminating transition metal ion perchlorates. The percentage change in the intensity of λ_{max} of the excimer band of **S2** in the presence of 10 equivalents of a perchlorate other than copper $[S2 + M^{n+}(ClO_4^-)_n]$, is shown as the orange bars in Figure 8. Alongside these, in blue is the further quenching resulting from addition of 10 equivalents of copper perchlorate to the same samples $[S2 + M^{n+}(ClO_4^-)_n + Cu(ClO_4)_2]$. A comparison of the results in lane 1 (copper perchlorate) with those in lanes 2–9 show copper detection is maintained in the presence
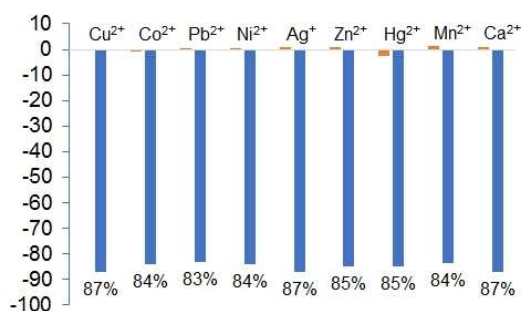
Figure 8. Percentage change in the intensity of maximum fluorescence emission [6 µM, λ_{ex} 348 nm], of the sensor **S2** (λ_{max} 480 nm) upon the addition of 10 eqs of metal perchlorates [**S2** + $M^{n+}(ClO_4^-)_n$] (orange bars), and upon the further addition of 10 eqs of copper perchlorate [**S2** + $M^{n+}(ClO_4^-)_n$ + $Cu(ClO_4)_2$] (blue bars).

Figure 9. a) Fluorescence spectra of **S2** (6 µM, MeCN) in the presence of 0–2 eqs of $Cu(ClO_4)_2$, b) Job's plot for **S2** in which the difference in fluorescence intensity multiplied by the mole fraction of the sensor ($\Delta F^*\chi_H$) at the λ_{max} was plotted against the mole fraction of the sensor (fitted to a curve $R^2 = 0.9910$). c) Benesi-Hildebrand plot of **S2** (6 µM MeCN) with $Cu(ClO_4)_2$ (0–2 eqs) (intercept = 0.0026, slope = -8×10^{-8}, fitted to a straight line $R^2 = 0.9887$). d) Stern-Volmer plot for **S2** (6 µM, MeCN) in which the fluorescence intensity ($\frac{I_0}{I}$) at λ_{max} was plotted against [$Cu(ClO_4)_2$] d(i), in the range 0–2 µM (fitted to a straight line, $R^2 = 0.9850$) and d(ii) in the range 0–12 µM (fitted to a curve, $R^2 = 0.9985$).

of foreign ions. Comparative binary interference studies indicate **S3** and **S4** also detect Cu(II) without interference from related ions, Figure S39.

A 1:1 stoichiometry for the interaction between each of **S2**-**S4** and copper ions in MeCN was determined from analyses of Job's plots,[29] and based on this stoichiometry, association constants, k_a, were determined by the Benesi-Hildebrand method[30] for **S1** (4.71×10^4 M^{-1}),[13] **S2** (3.25×10^4 M^{-1}), **S3** (2.96×10^4 M^{-1}) and **S4** (0.60×10^4 M^{-1}). The detection limits were measured[31] to be between 0.3–3.6 µM, this compares with the US EPA guideline that drinking water should not contain more than 1.3 mg copper per litre ($\sim 2 \times 10^{-5}$ M). Fluorescence quenching constants, K_{SV}, were estimated from Stern-Volmer plots;[32] the slope of the linear plots, for data collected in the range 0–2 µM, gives K_{SV} **S1** (4.47×10^4 M^{-1}),[13] **S2** (4.19×10^4 M^{-1}), **S3** (2.60×10^4 M^{-1}) and **S4** (1.03×10^4 M^{-1}). As Cu(II) concentration increased the plots better fitted to curves in keeping with the operation of both static and dynamic quenching mechanisms at higher analyte concentrations, Figures 9 and S40-42.

Even with the proviso that the complexes of Cu(II) should be more stable than those of chemically related metal ions,[33] the selectivity of **S1-S4** for Cu(II) over the other perchlorates studied remains remarkable. To probe the sensing mechanism electrochemical and NMR spectroscopic studies were undertaken. Electrochemical profiles, cyclic voltammetry (CV) and differential pulse voltammetry (DPV), were obtained for separate samples of sensor, **S**, analyte, **A**, and for mixed **S-A** samples. The chosen electrolyte was 0.1 M TBAPF$_6$ in acetonitrile. Solubility limitations at 1×10^{-3} M ruled out **S1** as the test case sensor and **S2** was chosen as the model compound. A potential window +1.7 to −1.0 V was employed to ensure all electrochemical activity of the samples could be observed within the operating potential limits for the selected solvent[34] and a platinum working electrode was selected to avoid the potentially problematic adsorption of the pyrene pendants at a glassy carbon electrode surface. When cyclic voltammetry was performed at scan rates of 100 and 50 mV s^{-1} some processes returned broad ill-defined redox waves and, thus, a scan rate of 20 mV s^{-1} was selected to provide clear peak definition for all
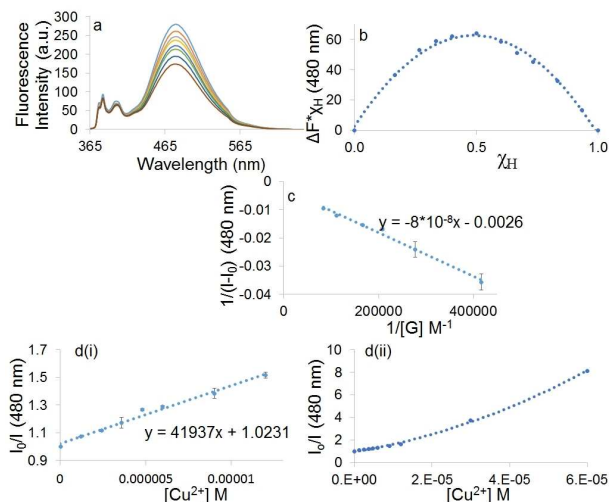
redox processes. Additionally, as steady-state profiles were not observed for either the sensor or the sensor- analyte solutions, the compared data are from the same CV cycle numbers.

The CV for the sensor only sample, **S2**, is dominated by an oxidation event, with a shoulder, A$_1$, at ca. +0.89 V leading into a sharp well defined peak, A$_2$, at $\sim$ +1.01 V; these processes likely describe a phenol oxidation,[35] Figure 10a. No redox peaks were observed in the cathodic run suggesting, as has been proposed for related 1,3-disubstituted calix[4]arenes, either irreversible oxidation,[35a] or the dominance of a higher rate chemical reaction which presents as an alternative once initial electron transfer has taken place.[35b]

DPV is a more sensitive tool than CV and two well-defined oxidation peaks, consistent with diquinone formation by sequential oxidation of the phenolic rings, are evident at 0.764 V (A$_1$, 2.29×10^{-6} A) and 0.880 V (A$_2$, 2.102×10^{-6} A) in the DPV of **S2**, Figure 11a. On the reverse sweep well-defined reduction peaks are observed at, 0.840 V (C$_1$, 5.29×10^{-7} A) and 0.984 V (C$_2$, 5.36×10^{-7} A), which describe the *coupled* diquinone-dihydroquinone reaction. The conversion of dihydroquinone to diquinone is kinetically more facile returning an A$_1$/C$_1$ (Ip,ox/Ip,red) peak current ratio of 4.3. The peak separation values for the A$_1$/C$_1$ and A$_2$/C$_2$ redox couples are 76 and 104 mV, respectively, and the process can be formally diagnosed as quasi-reversible. It is likely that the electrochemical oxidation of **S2** is a multistep process involving a series of proton and electron transfer steps (A$_1$ & A$_2$), nucleophilic attack by an advantageous water molecule, and a dealkylation step culminating in formation of a calixdiquinone (**S2-Q$_2$**) derivative.[35b]
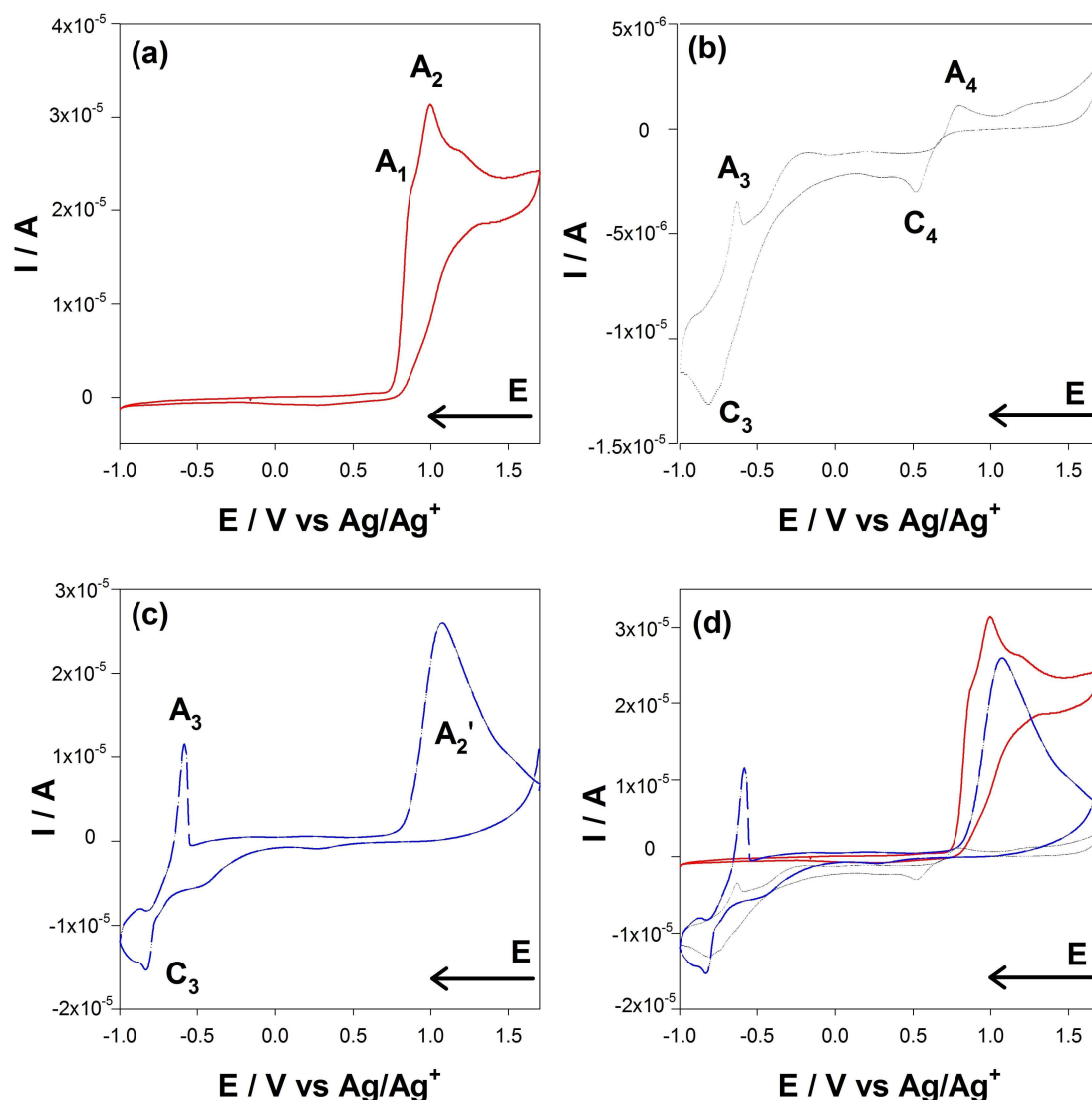
Figure 10. Typical cyclic voltammograms, obtained at a platinum working electrode, detailing the redox behaviour of **(a)** Sensor = **S2**, (red solid trace); **(b)** Analyte, **A** = Cu(ClO$_4$)$_2$, (black dotted trace); **(c) S2-A** sample, (blue dashed trace). Concentrations of each species, 1 × 10^{-3} M, supporting electrolyte, 0.1 M TBAPF$_6$ in MeCN, and scan rate, 20 mV s^{-1}; **(d)**. Comparative cyclic voltammograms, of those presented in Figure 10(a)–(c), with **S2**, (red solid trace), **A**, (black dotted trace) and **S2-A** samples, (blue, dashed trace).

The CV of the analyte sample, **A**, Cu(ClO$_4$)$_2$ includes a well-defined quasi-reversible Cu(II)/Cu(I) redox couple with Cu(II) to Cu(I) reduction, C$_4$, occurring at ~ +0.520 V, while the related Cu(I) to Cu(II) oxidation, A$_4$, was observed at ~ +0.800 V (ΔEP = 280 mV). The further reduction of Cu(II) to Cu^0, C$_3$, and the corresponding Cu^0 to Cu(II) stripping, A$_3$, processes were evident at ~-0.810 and −0.630 V, respectively, Figure 10b. As expected for copper electrochemistry in a non-ideal electrolyte this process is quasi-reversible, and returned a ΔE$_P$ value of 170 mV. The CV data from the **S2-A** solution displays several notable features.

Firstly, the shoulder and main peak, A$_1$ and A$_2$, representing the **S2** oxidation process merge into a single broader oxidation wave, A$_2$′. This ~60 mV anodic shift for sensor oxidation, A$_2$′, Figure 10d, is less than that typically expected following association with a divalent cation. The small magnitude of the

shift is suggestive of binding to a lesser charged ion, i.e. Cu(I) rather than Cu(II).[36] Secondly, a comparison of the copper stripping peak in the CV recorded for the **S2-A** sample, A$_3$, shows an enhanced definition and a notable increase in current magnitude with respect to the corresponding peak in the **A** only sample, Figures 10b–d. The increased deposition of copper from the **S2-A** sample and the lack of a discernible Cu(II) Cu(I) reduction peak, C$_4$, Figure 10c–d, and S44, conspire to suggest an increased availability of Cu(I), in the bound form, in the **S2-A** sample. The CV study thus implies Cu(II) may partake in a homogeneous reaction with **S2** to produce Cu(I) which is the guest of a redox generated calix[4]diquinone, **S2-Q$_2$**.

DPV data corroborates with the CV analysis and the oxidation profile of the equimolar **S2-A** sample is markedly different from that of either species alone, Figure 11b. Immediately following analyte addition a number of significant
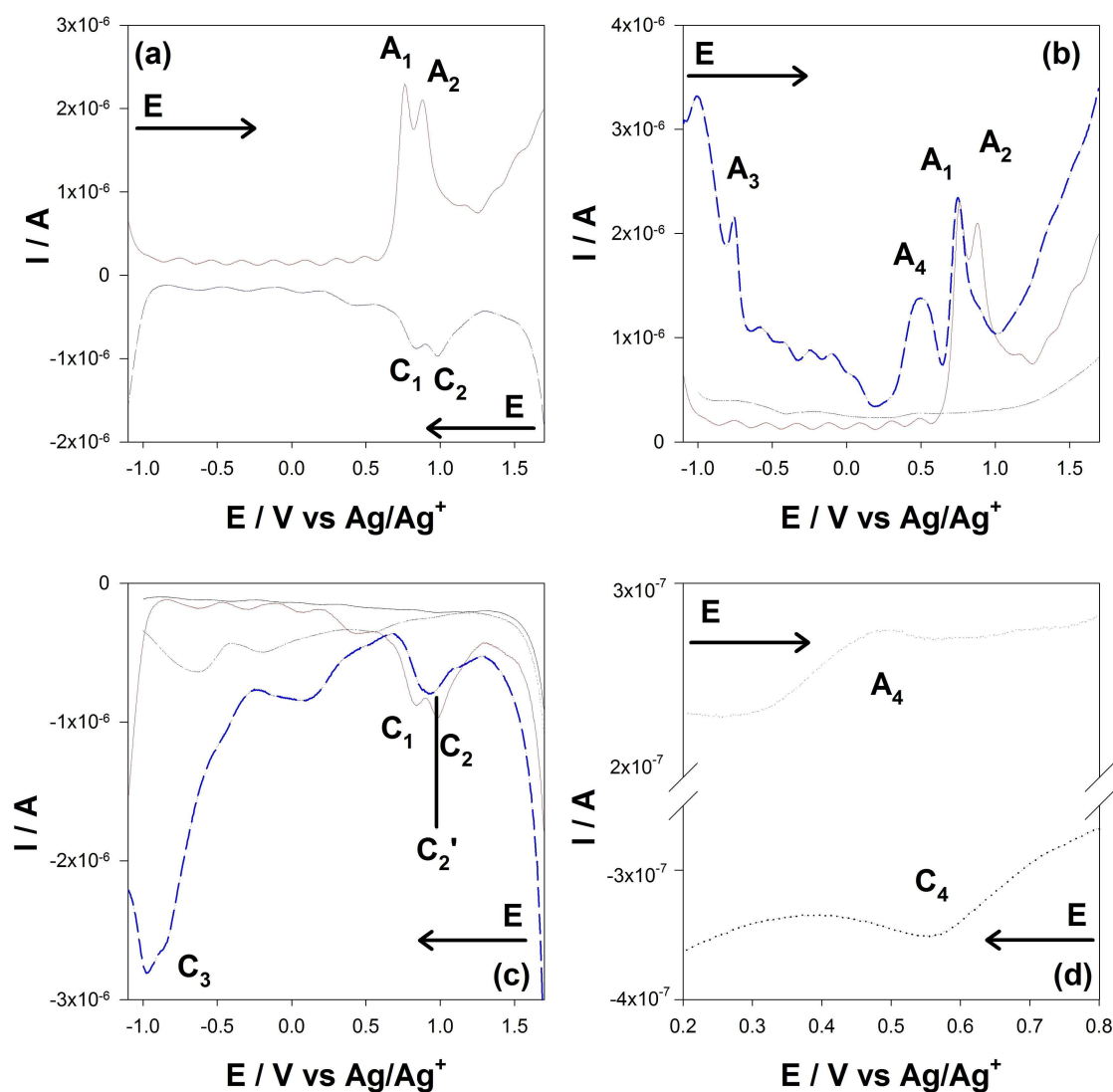
Figure 11. Typical DPVs, at a platinum electrode in 0.1 M TBAPF$_6$ in MeCN for 1×10^{-4} M samples of Sensor **S2**; Analyte, **A** = Cu(ClO$_4$)$_2$ and equimolar **S2-A** mixtures. **(a)** **S2**, forward oxidation sweep (red solid trace) and reverse reduction sweep (blue trace dotted); **(b)** Oxidation profiles **A** (black dotted trace), **S2** (red solid trace), and **S2-A** (blue dashed trace): **(c)** Reduction profiles **A** (black dotted trace), **S2** (red solid trace), **S2-A** (blue dashed trace), and MeCN (black solid trace): **(d)** Enlarged Cu(II)/(I) oxidation, A$_4$, and Cu(I)/Cu(II) reduction, C$_4$, regions in the **A** only sample.

changes are noted. The A$_2$ oxidation wave is seen to disappear suggesting an instantaneous homogeneous catalytic reaction between Cu(ClO$_4$)$_2$ and one of the phenolic rings on the sensor. It is also evident that the magnitude of the Cu(I) oxidation wave, A$_4$, is significantly enhanced in the **S2-A** sample compared to that in the analyte only solution, Figure 11d. As may be expected from an **S2-A** reaction generating Cu(I) in solution, the copper stripping peak, A$_3$, is also of much larger magnitude in the presence than in the absence of the sensor. The most obvious differences between the reduction profiles of an **S2-A** sample and individual samples of **S2** and **A** are that the two distinct waves associated with the reduction of both quinone moieties of **S2**, C$_1$, & C$_2$, are replaced by a single broader wave, C$_2$′, Figure 10c. In addition, the copper deposition process, C$_3$, visible as a broad wave at −0.632 V (2.050×10^{-7} A) in the **A** only sample is much sharper and better defined in the mixed sample. The observed changes, indicating more facile

Cu^0 deposition from the **S2-A** mixture than from Cu(ClO$_4$)$_2$ alone could be attributed to an immediate sensor promoted, homogeneous production of Cu(I) from Cu(ClO$_4$)$_2$. However, if the availability of Cu(I) in solution were to have increased by this mechanism a more positive reduction potential would have been expected to be returned for the kinetically more facile Cu (I)/Cu^0 deposition process. We suggest the observed requirement for additional potential to power the deposition process from the **S2-A** sample is consistent with an intermediate species with Cu(I) ions loosely bound to an oxidised sensor. The enhanced Cu^0/Cu(II) stripping process, C$_3$, in the presence of sensor further supports this proposed mechanism, Figure 11c.

^{1}H NMR spectroscopic studies (500 MHz, 0.54 mM, CD$_3$CN: CDCl$_3$, 4:1, v/v) of the sensor-analyte interactions validate copper perchlorate detection by a mechanism involving Cu(II) *consumption* for **S1**–**S3**. Only in the case of the **S4**-Cu(II) samples did the expected difficulties associated with paramagnetic Cu(II)
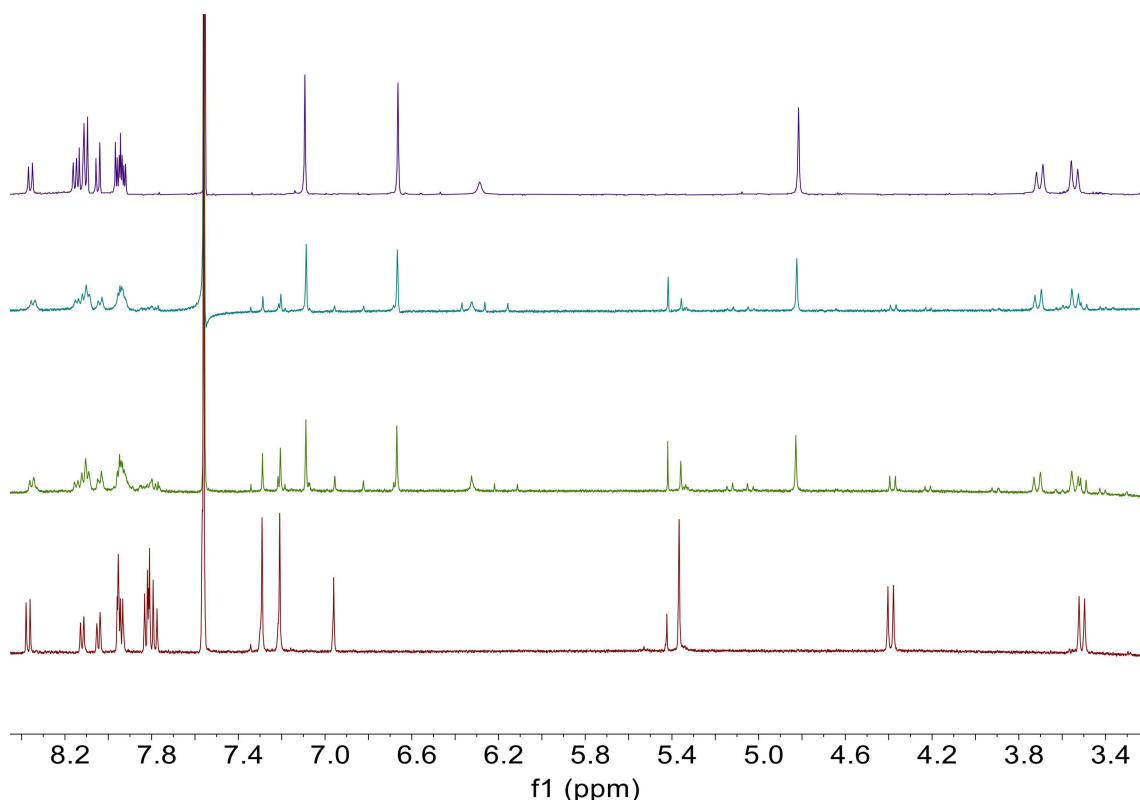
Figure 12. ^{1}H NMR spectra (500 MHz) of 0.54 mM samples of **S1** (CD$_3$CN:CDCl$_3$, 4:1, v/v) at 25 °C in the region between 8.50 and 3.00 ppm with no analyte (maroon), one equivalent of Cu(ClO$_4$)$_2$ (green); two equivalents of Cu(ClO$_4$)$_2$ (turquoise) and the ^{1}H NMR spectrum (500 MHz) of isolated **S1-Q$_2$** (CD$_3$CN:CDCl$_3$, 4:1, v/v) (purple).

ions present. Significant differences between the data reported for **S1** in this work and that which we previously recorded[13] emphasise the importance of sample preparation. Thus, the **S-A** solutions must be thoroughly mixed and all measurements made under the same conditions.

The **S1-S3**/Cu(ClO$_4$)$_2$ ^{1}H NMR spectra, remarkably well resolved and incompatible with the presence of a paramagnetic Cu(II) complex, suggest a mixture including one dominant new species and a varying number of more minor species as well as unchanged sensor, Figures 12 and S45–47. In each case a new pair of calix-ArH, with lower chemical shift and with Δ_δ's greater than those of the free sensors [0.24–0.44 ppm compared to <0.1 ppm] can be seen. After the addition of two analyte equivalents the relative integrals of new calix-ArH to those of the free sensors rose to ~6:1, 1:1 and 0.8:1 for **S1**, **S2** and **S3** respectively. Analyte induced shielding of the lower rim methylene *exo* protons of **S1-3** [up to ~0.6 ppm] and of the calix-OCH$_2$-isoxazole methylene protons was also noted for **S1** (~0.52 ppm) and **S2** (~0.37 ppm). The ethylene chain protons are also shielded in the **S3**-Cu(ClO$_4$)$_2$ sample.

Copper ions have an affinity for oxa- and aza-ligands hence the lower rim hydroxy groups and the heterocyclic nuclei are potentially valuable cation binding motifs. The spectra of the **S-A** samples were closely examined for diagnostic changes to the OH and isoxazole-H signals. The coincident resonance of the phenolic-OH with a multiplet pyrene-H signal made it impossible to track analyte-induced changes to this signal for **S1**.

However, in **S2** and **S3** the equivalent proton resonates distinct from any other. Following analyte addition it persists, albeit with relative intensity diminished in line with the fraction of free sensor in the sample. In parallel, a progressive decrease in the intensity of the parent heterocyclic-H signal was noted alongside the emergence of a new, upfield broad isoxazole-H signal [$\Delta\delta$ 0.12–0.63 ppm]. For all **S-A** samples the relative integral of the new isoxazole-H to the new calix-ArH signals was 1:2:2.

The loss of all semblance of the fine structure of the **S4** pyrene-H resonances is an immediate consequence of Cu(ClO$_4$)$_2$ addition. Interestingly, whilst most other signals were also broad the analyte induced a relative sharpening of the calix-ArH signals, however, no substantial change to chemical shift was noted for any proton, Figure S48. The site-specific broadening suggests paramagnetic Cu(II) ions may engage with **S4** in the vicinity of the pendant aromatic nuclei. The contrasting influence of copper perchlorate on the NMR spectra of **S1-S3** with **S4** is compatible with sensing by two independent mechanisms.

As voltammetric and ^{1}H NMR studies implicate Cu(II) *consumption* in the sensing process, roles for potential redox generated Cu(I) ions were probed. Spectrofluorometric studies clearly show that **S1** does not sense Cu(I) either directly or indirectly; the fluorescence profile of **S1** did not change on the addition of 50 equivalents of Cu(PF$_6$), neither did the addition of 10 equivalents of Cu(PF$_6$) to a sample of **S1** plus 10 equivalents
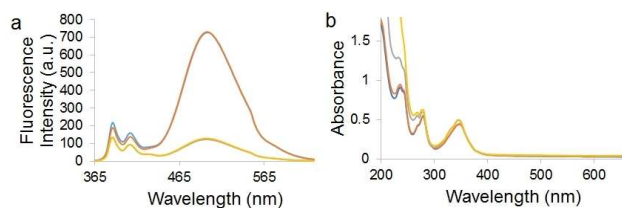
Figure 13. a) Fluorescence emission spectra (λ_{ex} 348 nm) and (b) absorption spectra of **S1**, in 6 μM, MeCN) with no additive (**S1**, blue); with 50 eqs of Cu (PF$_6$) (**S1-Cu(I)**, orange), with 10 eqs of Cu(ClO$_4$)$_2$ (**S1-Cu(II)**, grey) and with 10 eqs of Cu(ClO$_4$)$_2$ plus a further 10 eqs of Cu(PF$_6$)$_2$ (**S1-Cu(I)Cu(II)**, yellow).

of copper perchlorate initiate any further quenching, Figure 13a.

The structural changes to **S1** upon Cu(II) addition, so evident from NMR and fluorescence spectroscopy, are not detectable from UV–vis absorption measurements. UV data for **S1**, **S1-Cu(I)**, **S1-Cu(II)** and **S1Cu(II)Cu(I)** samples are practically identical. In particular, none of the **S1-Cu** samples provide support for a new metal ligand charge transfer band which would be expected should a Cu(I)-phenoxy radical complex be present,[14–15] Figure 13b.

To determine the nature of the calixarene oxidation product (s) a chemical reaction was conducted between **S1** and Cu (ClO$_4$)$_2$. Dropwise addition of an acetonitrile solution of the perchlorate salt (10 eqs) to an ice-cold solution of **S1** in MeCN/ CHCl$_3$ resulted in a change from colourless to pale brown. After stirring overnight at rt, work-up involving an NH$_4$Cl wash, and purification by column chromatography a symmetrical structure identified as the calixdiquinone **S1-Q$_2$** was isolated, Scheme 3. The structure of **S1-Q$_2$** is supported by high resolution mass spectrometry (HRMS) data which concurs with the expected
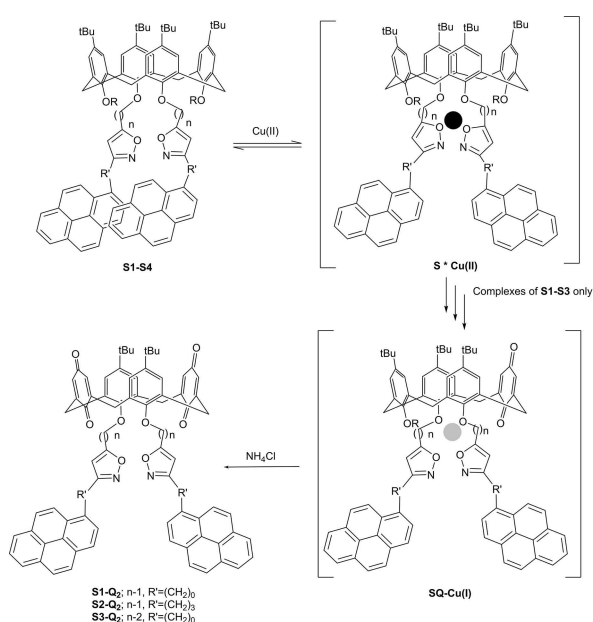
mass. Resonances at 7.10 and 6.66 ppm in the ^{1}H NMR spectrum represent calix-ArH and calixdiquinone ArH, Figure 12. In the ^{13}C NMR spectrum two quinone carbon resonances are found at ~188 and 186 ppm significantly downfield of the respective quaternary carbon atoms in the parent **S1** molecule. Small scale experiments in NMR tubes show **S2** and **S3** respond to excess Cu(ClO$_4$)$_2$ in a parallel manner. In each case one symmetrical product can clearly be seen emerging from the crude reaction mixture, Figure S52. TLC-MS analysis of the solution of **S3** plus excess Cu(ClO$_4$)$_2$ after an NH$_4$Cl wash and filtration through a silica pad shows m/z 1177 consistent with the sodium ion of the calixdiquinone, **S3-Q$_2$**. Oxidative routes to calixdiquinones generally involve thallium[37] or lead[38] reagents and whilst Chung's Fe^{3+} sensing by a 1,2,4-oxadiazole-substituted calixarene provides precedence for redox mediated, transition metal ion sensing promoting calix[4]diquinone generation,[17] as far as we can tell this work represents the first isolation of a Cu(II) generated calix[4]diquinone.

The response of **S1-S4** to Cu(II) was highly dependent on the nature of the counterion. The four sensors responded consistently to the acetate, nitrate or chloride salts causing ~12, 59 and 69% quenching respectively, Figure S43. Whilst some sensing systems do not involve counterion participation, e.g. Cu (II) binding by organosilicon complexes[39] there is precedence for an anion dependence on cation sensing across a range of mechanisms. For example, ion pairing is important in crown ether lead sensing,[40] it is also suggested that anion effects can be due to their pH[41] and significantly Cu(II) detection by means of oxidation behaviour towards a ferrocene unit is reported to be profoundly influenced by the counterion.[42] The apparent anomaly between the limited response of the lower rim substituted **S4** (~27% fluorescence quenching) and the unsubstituted analogues **S1-S3** (~83–100% fluorescence quenching) to 100 equivalents of Cu(ClO$_4$)$_2$ is reconcilable by consideration of sensing by two distinct mechanisms. It is likely that, in all cases, an initial Cu(II) complexation involving the isoxazole nuclei of **S1-S4** causes sensor quenching via energy- or electron transfer, and that this event is singularly responsible for the fluorescence turn-off elicited by **S4** which is not a substrate for calixdiquinone generating redox chemistry. Thus, for **S4** the sensitivity towards copper salts is solely dependent on a counterion sensitive **S+A⇌S-A** equilibrium position with the limited sensitivity towards the perchlorate salt being suggestive of a left lying equilibrium. The vastly enhanced response of **S1-S3** to Cu(ClO$_4$)$_2$ can be accommodated by assuming an initial complexation brings the Cu(II) ion into the proximity of the phenolic-OH groups and facilitates an irreversible redox reaction culminating in calixdiquinone **S-Q$_2$** generation. The conformational features of the calixdiquinones do not permit intramolecular excimer formation and are therefore responsible for the definitive Cu(II) induced fluorescence turn-off.

Conclusion

A quench of the fluorescence emission band of calix[4]arenes substituted on the upper rim with *t*Bu groups and on the lower

Scheme 3. Proposed mechanism for fluorescence turn-off Cu(II) sensing by **S1-S4**, culminating in the formation of calixdiquinones **S1-Q$_2$**, **S-Q$_2$** and **S3-Q$_2$** from **S1-S3**, and an **S*Cu(II)** complex from **S4**.

rim with isoxazolo-pyrene pendants accompanies selective and sensitive detection of industrially and biologically relevant Cu(II) ions. The sensors, **S1-S3**, with lower rim phenolic groups are more sensitive to copper perchlorate than is **S4** which is fully substituted on the small rim. ^{1}H NMR spectroscopic studies support the classification of **S4** as a *traditional* chelation type chemosensor detecting Cu(II) by a reversible complexation. The sensitivity of **S4** towards a particular copper salt, as determined by spectrofluorometric data, is dependant only on the equilibrium position of the **S4 + A $\rightleftharpoons$ S4-A** event. In contrast, voltammetric studies, NMR and UV/Vis spectroscopy data support characterisation of **S1-3** as chemodosimeters where copper ions are sensed by an irreversible redox reaction facilitated by an initial reversible chelation event. In all cases the stoichiometry of the interaction between copper perchlorate and the sensor was 1:1 and detection limits were in the micromolar or sub-micromolar range. In conclusion, we have demonstrated differential sensing of Cu(II) via two different mechanisms with the fully substituted calixarene, **S4**, acting as a chemosensor, and the 1,3-disubstituted calixarenes **S1-S3** behaving as chemodosimeters.

Experimental Section

General Information: Standard reagents were supplied by Alfa Aesar, TCI Europe or Sigma Aldrich and were used without further purification. HPLC grade solvents were used as received. Analytical TLC was performed on pre-coated silica gel 60 F$_{254}$ plates from Merck. All plates were visualised by UV irradiation. Flash chromatography was performed using silica gel 40–63 μM, 60 Å. Electrospray (ESI) mass spectra were carried out on an Agilent Technologies 6410 Time of Flight LC/MS. NMR spectra were recorded on a Bruker Avance spectrometer at 25 °C except where otherwise stated. NMR spectra were recorded in CDCl$_3$ unless otherwise stated. Chemical shifts are reported in ppm downfield from TMS as standard. ^{1}H and ^{13}C NMR were recorded at 500 and 125 MHz respectively unless otherwise stated. UV-Vis spectra were recorded with a UNICAM UV500 UV-Visible Spectrometer. Fluorescence spectra were recorded with a Jasco FP-6300 spectrofluorometer operating in emission mode. Excitation and emission bandwidths were set at 2.5 nm. All fluorescence experiments were carried out in triplicate. Infrared spectra were recorded as KBr discs using a Perkin Elmer system 2000 FT-IR spectrophotometer. Melting point analyses were carried out using a Stewart Scientific SMP 11 melting point apparatus. Sodium hydride (NaH) was obtained as a 60% dispersion in mineral oil from Sigma Aldrich; immediately prior to use the mineral oil covering was removed using petroleum ether under a N$_2$ atmosphere. The stripped NaH was retained in an inert atmosphere and used immediately.

We did not experience any problem during this work, however, it must be noted that perchlorate salts of metal ions are potentially explosive, they must be manipulated with care and used only in small quantities.

1-Pyrenebutanaldoxime, 3. Approach (i): 1-Pyrenebutanal (694 mg, 2.55 mmol, 1 eq) was dissolved in EtOH (20 mL) in a scientific MW vessel. Hydroxylamine hydrochloride (266 mg, 3.82 mmol, 1.5 eq) and pyridine (302 mg, 3.82 mmol, 1.5 eq) were added. The resulting mixture was heated to 125 °C in a scientific MW (t = 1 hr, P$_{max}$ = 300 W). Following cooling, water (10 mL) was added to the solution. The organic layer was extracted with

chloroform (30 mL), dried over anhydrous magnesium sulphate and the solvent removed under reduced pressure to yield the crude product as a dark yellow solid which was purified by flash column chromatography (SiO$_2$, petroleum ether:DCM; 6:4, v/v) to produce 1-pyrenebutanenitrile, **4** (46%) and 1-pyrenebutanaldoxime (43%), as a 2:3 ratio of *E*-:*Z*-isomers in CDCl$_3$ at rt. **Approach (ii)**: 1-Pyrenebutanal (688 mg, 2.53 mmol, 1 eq) was dissolved in MeOH:H$_2$O (60 mL, 11:1, v/v), hydroxylamine hydrochloride (351 mg, 5.06 mmol, 2 eq) and sodium acetate trihydrate (688 mg, 5.06 mmol, 2 eq) were added. The resulting solution was heated to reflux for 3 hrs. Following cooling, addition of water (50 mL) to the solution induced formation of a pale yellow ppt which was collected and dried to yield the pure oximes in a 1:1.8 mixture of *E*- and *Z*-isomers (92%). **Oxime 3**: m.p. = 114–117 °C; ^{1}H NMR: δ = 8.29–8.24 (m, 1H, ArH), 8.20–8.15 (m, 2H, ArH), 8.15-8.09 (m, 2H, ArH), 8.07-7.96 (m, 3H, ArH), 7.90–7.85 (m, 1H, ArH), 7.52 (t, J = 5.9 Hz, 0.4 H, C$\underline{H}$NOH *E*-isomer), 7.37 (br s, 0.6 H, NO$\underline{H}$ *Z*-isomer), 7.07 (br s, 0.4 H, NO$\underline{H}$ *E*-isomer), 6.81 (t, J = 5.5 Hz, 0.6 H, C$\underline{H}$NOH *Z*-isomer), 3.44–3.38 (m, 2H, pyr-C$\underline{H}_2$), 2.60–2.53 (m, 1.2H, C$\underline{H}_2$CHNOH *Z*-isomer), 2.41–2.34 (m, 0.8H, C$\underline{H}_2$CHNOH, *E*-isomer), 2.12–2.04 (m, 2H, pyr-CH$_2$C$\underline{H}_2$); ^{13}C NMR: δ = 152.0 (C$\underline{H}$NOH), 135.8, 135.8, 131.4, 130.9, 130.0, 128.7, 128.6 (7×qC), 127.5, 127.4, 127.4, 127.3, 127.3, 126.7, 125.9 (7×C$\underline{H}$), 125.1, 125.0 (2×qC), 125.0 (C$\underline{H}$), 125.0 (qC), 124.8, 124.8, 124.8, 123.3, 123.2 (5×C$\underline{H}$), 33.2, 32.8, 29.3, 28.4, 28.2, 24.9 (6×C$\underline{H}_2$); IR (KBr): 3397, 3210, 2928, 2858, 1663, 1435, 844 cm^{-1}; HRMS (ESI): calcd for C$_{20}$H$_{17}$NO + Na: 310.1202 [M + Na]$^+$; found 310.1207 (diff ppm −1.61). **Nitrile 4**: m.p. = 90–93 °C; ^{1}H NMR: δ = 8.24 (d, J = 9.3 Hz, 1H, ArH), 8.22–8.17 (m, 2H, ArH), 8.17–8.11 (m, 2H, ArH), 8.08–7.99 (m, 3H, ArH), 7.88 (d, J = 7.8 Hz, 1H, ArH), 3.53 (t, J = 7.5 Hz, 2H, pyr-C$\underline{H}_2$), 2.41 (t, J = 7.0 Hz, 2H, C$\underline{H}_2$CN), 2.27–2.19 (m, 2H, pyr-CH$_2$C$\underline{H}_2$); ^{13}C NMR: δ = 133.7 (1-pyr-qC), 131.4, 130.8, 130.4, 128.7 (4×qC), 127.8, 127.4, 127.3, 127.1, 126.0, 125.2 (6×C$\underline{H}$), 125.2 (qC), 125.0, 124.9 (2×C$\underline{H}$), 124.9 (qC), 122.7 (C$\underline{H}$), 119.6 (C$\underline{N}$), 32.0 (pyr-C$\underline{H}_2$), 27.2 (C$\underline{H}_2$CN), 16.8 (C$\underline{H}_2$CH$_2$CN); IR (KBr): 3049, 2246, 1601, 1433, 843 cm^{-1}; HRMS (ESI): m/z calcd for C$_{20}$H$_{15}$N + Na: 292.1097 [M + Na]$^+$; found 292.1102 (diff ppm −1.71).

5,11,17,23-*tetra-tert*-Butyl-25,27-bis[(3-(3-(pyren-1-yl)propyl) isoxazol-5-yl)methyl]-26,28-dihydroxycalix[4]arene, S2 The oxime **3** (476 mg, 1.66 mmol, 6 eq) was dissolved in DCM (60 mL), NCS (332 mg, 2.49 mmol, 9 eq) was added and the solution was allowed to stir at rt for 1 hr. The alkyne **1** (200 mg, 0.28 mmol, 1 eq) was added and the resulting solution was heated to reflux. NEt$_3$ (502 mg, 694 μL, 4.96 mmol, 18 eq), dissolved in DCM (306 μL) was added to the refluxing solution over 17 hrs using a syringe pump operating at 1 μL/min. Following cooling, the organic extracts were washed with water (2×30 mL), dried over anhydrous sodium sulphate and the solvent removed under reduced pressure to yield the crude product which was purified by flash column chromatography (SiO$_2$, DCM; 100%) to yield the pure product as an off-white solid, 49%, m.p. = 117–120 °C; ^{1}H NMR: δ = 8.18 (d, J = 9.2 Hz, 2H, ArH), 8.13–8.09 (m, 2H, ArH), 8.08–8.05 (m, 2H, ArH), 8.03–7.98 (m, 4H, ArH), 7.98–7.91 (m, 6H, ArH), 7.78 (d, J = 7.7 Hz, 2H, ArH), 7.03 (s, 4H, calix-ArH), 6.72 (s, 4H, calix-ArH), 6.62 (s, 2H, 2×OH), 6.32 (s, 2H, 2×isox-$\underline{H}$), 4.97 (s, 4H, OC$\underline{H}_2$), 4.15 (d, J = 13.3 Hz, 4H, calix-CH methylene bridge), 3.34 (t, J = 6.9 Hz, 4H, pyr-CH$_2$), 3.24 (d, J = 13.3 Hz, 4H, calix-CH methylene bridge), 2.75 (t, J = 7.2 Hz, 4H, pyr-CH$_2$CH$_2$C$\underline{H}_2$), 2.22–2.12 (m, 4H, pyr-CH$_2$C$\underline{H}_2$), 1.27 (s, 18H, *t*-butyl C$\underline{H}_3$), 0.89 (s, 18H, *t*-butyl C$\underline{H}_3$); ^{13}C NMR: δ = 167.5, 163.7, 150.4, 149.5, 147.6, 141.8, 135.8, 132.2, 131.4, 130.9, 129.9, 128.7, 127.7, 127.7 (13×qC), 127.5, 127.4, 127.3, 126.6, 125.8, 125.7, 125.2 (7× C$\underline{H}$), 125.1, 125.0 (2×qC), 124.8, 124.8, 123.3 (3×C$\underline{H}$), 103.5 (isox-C$\underline{H}$), 68.3 (OC$\underline{H}_2$), 33.9 (*t*-butyl qC), 33.8 (*t*-butyl qC), 32.8 (pyr-C$\underline{H}_2$), 31.7 (*t*-butyl C$\underline{H}_3$), 31.5 (calix-CH$_2$ methylene bridge), 30.9 (*t*-butyl C$\underline{H}_3$), 30.0 (isox-CH$_2$C$\underline{H}_2$), 25.9 (isox-C$\underline{H}_2$); IR (KBr): 3416, 2959, 1603, 1485, 1202, 1018, 848 cm^{-1}. HRMS (ESI): calcd for C$_{90}$H$_{90}$N$_2$O$_6$ + K: 1333.643 [M + K]$^+$; found 1333.6435 (diff ppm −0.37).

5,11,17,23-tetra-tert-Butyl-25,27-bis(but-3-ynyloxy)-26,28-dihy-droxycalix [4]arene, 2[19] 4-*tert*-Butylcalix[4]arene (1.000 g, 1.54 mmol, 1 eq) was dissolved in anhydrous acetonitrile (30 mL), potassium carbonate (1.064 g, 7.70 mmol, 5 eq) was added and the solution was allowed to stir for 1 hr at rt to allow for deprotonation. 4-Bromo-1-butyne (0.860 g, 6.47 mmol, 4.2 eq) in anhydrous acetonitrile (10 mL) was added dropwise over 30 min and the resulting solution was heated to reflux for 24 hrs. The solution was then allowed to cool, filtered over celite to remove any insoluble impurities and the filtrate was concentrated under vacuum. 2 M HCl (20 mL) was added and the mixture was extracted with DCM, washed with water (30 mL×2), brine (30 mL), dried over MgSO$_4$ and the solvent removed under reduced pressure to yield a white solid. The crude product was purified by flash column chromatography (SiO$_2$, Pet. Ether:EtOAC, 10:0.5, v/v) to give the pure product as a bright white solid, 36%, m.p.=232–234 °C. ^{1}H NMR spectroscopic data corresponded to that found in the literature.

5,11,17,23-Tetra-tert-Butyl-25,27-bis[(3-(pyren-1-yl)isoxazol-5-yl) ethyl]- 26,28-dihydroxycalix[4]arene, S3 The alkyne **2** (100 mg, 0.13 mmol, 1 eq) was dissolved in EtOH (40 mL), 1-pyrenecarbaldox-ime (130 mg, 0.53 mmol, 4 eq) and Ch–T (65 mg, 0.27 mmol, 2 eq) were added and the solution was allowed to stir at reflux. Further portions of Ch–T (65 mg, 0.27 mmol, 2 eq) were added at t=3 and t=6 hrs. The resulting solution was then allowed to stir for 18 hrs at reflux. Following cooling, water (20 mL) was added to the solution. The organic layer was extracted with chloroform (40 mL), washed with 5% NaOH (30 mL), dried over anhydrous magnesium sulphate and the solvent removed under reduced pressure to yield the crude product which was purified by flash column chromatography (SiO$_2$, DCM; 100%). The pure product was obtained as a white solid by crystallisation from EtOH:DCM (2:1, v/v), 49%, m.p.=162 - 165 °C; ^{1}H NMR: δ=8.45 (d, J=9.5 Hz, 2H, ArH), 8.17– 8.11 (m, 4H, ArH), 8.09–8.02 (m, 8H, ArH), 7.97–7.92 (m, 2H, ArH), 7.58 (d, J=9.5 Hz, 2H, ArH), 7.13 (s, 4H, calix-ArH), 6.88 (s, 2H, isox-H), 6.78 (s, 2H, OH), 6.73 (s, 4H, calix-ArH), 4.03 (d, J=13.0 Hz, 4H, calix-CH methylene bridge), 3.95 (t, J=6.1 Hz, 4H, OCH$_2$), 3.25 (d, J=13.0 Hz, 4H, calix-CH methylene bridge), 2.76 (t, J=6.2 Hz, 4H, OCH$_2$CH$_2$), 1.38 (s, 18H, t-butyl CH$_3$), 0.90 (s, 18H, t-butyl CH$_3$). ^{13}C NMR: δ=169.4, 163.2, 150.6, 149.4, 147.3, 141.7, 132.1, 132.0, 131.2, 130.8, 129.0, 128.3, 128.3, 127.7, 127.4, 127.3, 126.0, 125.6, 125.4, 125.3, 125.2, 124.9, 124.7, 124.6, 124.4, 124.2, 105.1 (isox-CH), 72.7 (OCH$_2$), 33.94 (t-butyl qC), 33.89 (t-butyl qC), 31.8 (t-butyl CH$_3$), 31.5 (calix-CH$_2$ methylene bridge), 30.9 (t-butyl CH$_3$), 27.2 (OCH$_2$CH$_2$); IR (KBr): 3416, 2959, 1603, 1485, 1202, 848 cm^{-1}. HRMS (ESI): calcd for C$_{86}$H$_{82}$N$_2$O$_6$+Na: 1261.6065 [M+Na]$^+$; found 1261.6039 (diff ppm −2.06).

5,11,17,23-tetra-tert-Butyl-25,27-bis[(3-(pyren-1-yl)isoxazol-5-yl) methyl]-26,28-dimethoxycalix[4]arene, S4 Approach (i). S1 (50 mg, 0.04 mmol, 1 eq) was dissolved in DMF (5 mL), NaH (30 mg, 1.23 mmol, 30 eq) was added and the resulting solution was stirred at rt for 15 mins. MeI (117 mg, 0.83 mmol, 20 eq) was added and the mixture allowed to stir at rt for 24 hrs. H$_2$O (10 mL) was added and the organic layer was extracted with DCM (20 mL), dried over anhydrous MgSO$_4$ and the solvent removed under reduced pressure to yield an off-white solid which was triturated with MeOH to yield the pure product as a bright white solid, 62%, m.p.=273–276 °C. **Approach (ii).** S1 (80 mg, 0.06 mmol, 1 eq) was dissolved in acetone (25 mL), Cs$_2$CO$_3$ (645 mg, 1.98 mmol, 30 eq) was added and the resulting mixture was stirred at rt for 15 mins. MeI (187 mg, 1.32 mmol, 20 eq) was added and the mixture heated at reflux for 17 hrs. Following cooling, H$_2$O (20 mL) was added and the organic layer was extracted with DCM (20 mL), dried over anhydrous MgSO$_4$. The solvent removed under reduced pressure to yield an off-white solid which was triturated with MeOH to yield the pure product as a bright white solid, 71%, m.p.=273–276 °C. **S4**

presented in a 1:2.78 ratio of cone and paco conformers in CDCl$_3$ at 240 K. ^{1}H NMR (240 K) - paco conformer: δ=8.55 (d, J=9.3 Hz, 2H, pyr-H), 8.17–7.80 (m, 16H, pyr-H)*, 7.30 (s, 2H, calix-ArH), 7.14 (br s, 2H, calix-ArH)*, 7.00 (br d, J=2.4 Hz, 2H, calix-ArH), 6.82 (s, 2H, isox-H), 6.60 (br d, J=2.4 Hz, 2H, calix-ArH), 5.12 (d, J=12.4 Hz, 2H, OCH), 4.88 (d, J=12.3 Hz, 2H, OCH), 4.23 (d, J=12.9 Hz, 2H, calix-CH methylene bridge), 3.86 (d, J=14.1 Hz, 2H, calix-CH methylene bridge), 3.79 (d, J=14.1 Hz, 2H, calix-CH methylene bridge), 3.37 (s, 3H, OCH$_3$), 3.34 (s, 3H, OCH$_3$), 3.20 (d, J=13.2 Hz, 2H, calix-CH methylene bridge), 1.34 (s, 9H, t-butyl CH$_3$), 1.11 (s, 9H, t-butyl CH$_3$), 1.07 (s, 18H, t-butyl CH$_3$); ^{1}H NMR (240 K) – cone conformer: δ=8.33 (d, J=9.3 Hz, 2H, cone pyr-H), 8.17–7.80 (m, 14H, pyr-H)*, 7.69 (d, J=8.9 Hz, 2H, cone pyr-H), 7.14 (br s, 4H, calix-ArH)*, 6.90 (s, 2H, isox-H), 6.57 (s, 4H, calix-ArH), 5.11 (s, 4H, OCH$_2$), 4.43 (d, J=12.6 Hz, 4H, calix-CH methylene bridge), 4.00 (d, 6H, OCH$_3$), 3.27 (d, J=12.7 Hz, 4H, calix-CH methylene bridge), 1.31 (s, 18H, t-butyl CH$_3$), 0.87 (s, 18H, t-butyl CH$_3$); (*denotes overlapping paco and cone ^{1}H NMR signals). ^{13}C NMR (240 K): conformer mixture; δ=169.1, 168.4, 162.9, 155.2, 155.0, 154.7, 152.8, 151.8, 145.4, 145.1, 144.8, 143.7, 135.3, 135.3, 133.0, 132.5, 132.4, 131.9, 131.8, 131.5, 130.7, 130.5, 130.2, 129.9, 128.7, 128.5, 128.3, 128.3, 128.0, 127.7, 127.0, 126.8, 126.7, 126.0, 125.8, 125.5, 125.4, 125.3, 125.1, 125.1, 124.6, 124.5, 124.4, 124.4, 124.3, 124.0. 123.6, 123.0. 122.7, 105.7, 105.2, 65.4, 60.5, 60.0, 57.9, 37.6, 34.1, 33.7, 33.7, 33.6, 31.6, 31.2, 30.9; IR (KBr): 2953, 1604, 1479, 1361, 1202, 1019, 845 cm^{-1}; HRMS (ESI): calcd for C$_{86}$H$_{82}$N$_2$O$_6$ + Na: 1261.6065 [M+Na]$^+$; found 1261.6105 (diff ppm −3.17).

Oxidation reactions of S1: 11,23-di-tert-Butyl-25,27-bis[(3-(pyren-1-yl)isoxazol-5-yl)methyl]-calix[4]diquinone S1-Q$_2$. To an ice-cooled solution of **S1** (30 mg) in MeCN/CHCl$_3$ (18 mL/9 mL) a solution of Cu(ClO$_4$)$_2$ (97.1 mg, 10 equivalents) in MeCN (18 mL) was added over a 5 minute period. The final solution, 0.54 mM **S1** in MeCN:CHCl$_3$ 4:1, was allowed to warm to room temperature and stirred overnight. The solvent was evaporated, the residue taken up in CH$_2$Cl$_2$ and washed firstly with water and then with sat NH$_4$Cl. After drying (anh. Na$_2$SO$_4$) and evaporation of the organics the brown residue was purified by flash column chromatography (CHCl$_3$:MeOH 99:1). Calixdiquinone **S1-Q$_2$** was isolated (14 mg, 50%).^{1}H NMR: δ=8.35 (d, J=8.9 Hz, 2H, ArH), 8.16–8.01 (m, 8H, ArH), 8.06–8.04 (d, J=8.9 Hz, 2H, ArH), 7.97–7.92 (m, 6H, ArH), 7.10 (s, 4H, calix-ArH), 6.66 (s, 4H, calixdiquinone-ArH), 6.28 (br s, 2H, 2× isox-H), 4.82 (s, 4H, OCH$_2$), 3.71 (d, J=14.8 Hz, 4H, calix-CH methylene bridge), 3.54 (d, J=14.8 Hz, 4H, calix-CH methylene bridge),1.24 (s, 18H, t-butyl CH$_3$); ^{13}C NMR: δ=188.7, 186.2 (2× quinone C=O), 168.1 (isoxazole-CO), 163.1 (isoxazole-CN), 152.9 (qCO-calixarene), 148.2 (qC-Calixdiquinone), 147.6, 132.6, 132.4 (ArCH -calixdiquinone), 131.3, 130.9, 130.8 (qC-calixarene) 129.1, 128.8, 127.7, 127.6 (qC-calixarene), 127.4 (ArCH-calixarene), 126.7, 126.1, 125.9, 125.1, 124.8, 124.7, 124.3, 123.4, 105.7 (isox-CH), 64.4 (OCH$_2$), 34.4 (qC t-butyl), 34.3 (Calix-CH$_2$-methylene bridge), 31.7 (t-butyl CH$_3$); HRMS (ESI): calcd for C$_{76}$H$_{58}$N$_2$O$_8$+Na; 1149.4085 [M+Na]$^+$; found 1149.4063 (diff ppm −1.19).

Acknowledgements

Conflict of Interest

The authors declare no conflict of interest.

[1] a) M. R. Awual, *Chem. Eng. J.* **2017**, *307*, 85–94; b) E. Tyrrell, C. Gibson, B. D. MacCraith, D. Gray, P. Byrne, N. Kent, C. Burke, B. Paull, *Lab Chip* **2004**, *4*, 384–390; c) T. Leelasattarathkul, S. Liawruangrath, M. Rayanakorn, B. Liawruangrath, W. Oungpipat, N. Youngvises, *Talanta* **2007**, *72*, 126–131; d) E. N. Zare, A. Motahari, M. Sillanpaa, *Environ. Res.* **2018**, *162*, 173–195; e) Q. Wei, R. Nagi, K. Sadeghi, S. Feng, E. Yan, S. J. Ki, R. Caire, D. Tseng, A. Ozcan, *ACS Nano* **2014**, *8*, 1121–1129; f) D. T. Sun, L. Peng, W. S. Reeder, S. M. Moosavi, D. Tiana, D. K. Britt, E. Oveisi, W. L. Queen, *ACS Cent. Sci.* **2018**, *4*, 349–356; g) M. A. Shenashen, S. Kawada, M. M. Selim, W. M. Morsy, H. Yamaguchi, A. A. Alhamid, N. Ohashi, I. Ichinose, S. A. El-Safty, *Nanoscale* **2017**, *9*, 7947–7959; h) H. Gomaa, S. El-Safty, M. A. Shenashen, S. Kawada, H. Yamaguchi, M. Abdelmottaleb, M. F. Cheira, *ACS Sustainable Chem. Eng.* **2018**, *6*, 13813–13825; i) M. A. Shenashen, S. A. El-Safty, E. A. Elshehy, *Analyst* **2014**, *139*, 6393–6405; j) S. A. El-Safty, M. A. Shenashen, *Sens. Actuators B* **2013**, *183*, 58–70; k) S. A. El-Safty, M. A. Shenashen, M. Ismael, M. Khairy, M. R. Awual, *Micro. Meso. Mater.* **2013**, *166*, 195–205.

[2] a) P. Verwilst, K. Sunwoo, J. S. Kim, *Chem. Commun.* **2015**, *51*, 5556–5571; b) Y.-W. Lin, C.-C. Huang, H.-T. Chang, *Analyst* **2011**, *136*, 863–871.

[3] a) Y. Guo, L. Zhang, S. Zhang, Y. Yang, X. Chen, M. Zhang, *Biosens. Bioelectron.* **2015**, *63*, 61–71; b) M. Lan, S. Zhao, S. Wu, X. Wei, Y. Fu, J. Wu, P. Wang, W. Zhang, *Nano Res.* **2019**, Ahead of Print.

[4] S. A. El-Safty, M. A. Shenashen, A. Shahat, *Small* **2013**, *9*, 2288–2296.

[5] J. Liu, Y. Lu, *J. Am. Chem. Soc.* **2007**, *129*, 9838–9839.

[6] K. Mariappan, P. N. Basa, V. Balasubramanian, S. Fuoss, A. G. Sykes, *Polyhedron* **2013**, *55*, 144–154.

[7] P. N. Basa, A. G. Sykes, *J. Org. Chem.* **2012**, *77*, 8428–8434.

[8] L. Liang, L. Zhao, X. Zeng, *J. Fluoresc.* **2014**, *24*, 1671–1677.

[9] J. Li, Z. Wang, G. Long, Q. Zhang, J. Li, S. Chen, P. Zhang, R. Ganguly, Y. Li, Q. Zhang, *Chem. Asian J.* **2016**, *11*, 136–140.

[10] Y. Xiang, A. Tong, *Luminescence* **2008**, *23*, 28–31.

[11] Q. Shen, S. Tang, W. Li, Z. Nie, Z. Liu, Y. Huang, S. Yao, *Chem. Commun.* **2012**, *48*, 281–283.

[12] a) A. Ramdass, V. Sathish, E. Babu, M. Velayudham, P. Thanasekaran, S. Rajagopal, *Coord. Chem. Rev.* **2017**, *343*, 278–307; b) J. Wu, B. Kwon, W. Liu, E. V. Anslyn, P. Wang, J. S. Kim, *Chem. Rev.* **2015**, *115*, 7893–7943.

[13] N. J. Maher, H. Diao, J. O'Sullivan, E. Fadda, F. Heaney, J. McGinley, *Tetrahedron* **2015**, *71*, 9223–9233.

[14] A. Senthilvelan, I. T. Ho, K.-C. Chang, G.-H. Lee, Y.-H. Liu, W.-S. Chung, *Chem. Eur. J.* **2009**, *15*, 6152–6160.

[15] I. T. Ho, J.-H. Chu, W.-S. Chung, *Eur. J. Org. Chem.* **2011**, *2011*, 1472–1481.

[16] K.-C. Chang, L.-Y. Luo, E. W.-G. Diau, W.-S. Chung, *Tetrahedron Lett.* **2008**, *49*, 5013–5016.

[17] Y.-J. Chen, S.-C. Yang, C.-C. Tsai, K.-C. Chang, W.-H. Chuang, W.-L. Chu, V. Kovalev, W.-S. Chung, *Chem. Asian J.* **2015**, *10*, 1025–1034.

[18] F. Heaney, *Eur. J. Org. Chem.* **2012**, 3043–3058.

[19] J. Bois, J. Espinas, U. Darbost, C. Felix, C. Duchamp, D. Bouchu, M. Taoufik, I. Bonnamour, *J. Org. Chem.* **2010**, *75*, 7550–7558.

[20] I. S. Kovalev, N. V. Slovesnova, D. S. Kopchuk, G. V. Zyryanov, O. S. Taniya, V. L. Rusinov, O. N. Chupakhin, *Russ. Chem. Bull.* **2014**, *63*, 1312–1316.

[21] L. J. O'Driscoll, D. J. Welsh, S. W. D. Bailey, D. Visontai, H. Frampton, M. R. Bryce, C. J. Lambert, *Chem. Eur. J.* **2015**, *21*, 3891–3894.

[22] B. Bi, K. Maurer, K. D. Moeller, *Angew. Chem.* **2009**, *48*, 5872–5874.

[23] J. E. Tonder, J. B. Hansen, M. Begtrup, I. Pettersson, K. Rimvall, B. Christensen, U. Ehrbar, P. H. Olesen, *J. Med. Chem.* **1999**, *42*, 4970–4980.

[24] a) S. L. Debbert, B. D. Hoh, D. J. Dulak, *J. Chem. Educ.* **2016**, *93*, 372–375; b) C. D. Gutsche, Editor, *Calixarenes: An Introduction, 2nd Edition*, Royal Society of Chemistry, **2008**.

[25] C. Jaime, J. De Mendoza, P. Prados, P. M. Nieto, C. Sanchez, *J. Org. Chem.* **1991**, *56*, 3372–3376.

[26] F. Benevelli, J. Klinowski, I. Bitter, A. Gruen, B. Balazs, G. Toth, *J. Chem. Soc. Perkin Trans. 2* **2002**, 1187–1192.

[27] R. Arce, E. F. Pino, C. Valle, I. Negron-Encarnacion, M. Morel, *J. Phys. Chem. A* **2011**, *115*, 152–160.

[28] a) T. M. Halasinski, F. Salama, L. J. Allamandola, *Astrophys. J.* **2005**, *628*, 555–566; b) O. Sahin, M. Yilmaz, *Tetrahedron* **2011**, *67*, 3501–3508.

[29] a) E. J. Olson, P. Buhlmann, *J. Org. Chem.* **2011**, *76*, 8406–8412; b) P. Job, *Ann. Chim.* **1928**, *9*, 113–203.

[30] H. A. Benesi, J. H. Hildebrand, *J. Am. Chem. Soc.* **1949**, *71*, 2703–2707.

[31] M. Zhu, M. Yuan, X. Liu, J. Xu, J. Lv, C. Huang, H. Liu, Y. Li, S. Wang, D. Zhu, *Org. Lett.* **2008**, *10*, 1481–1484.

[32] a) V. Singh, P. Srivastava, S. Prakash Verma, A. Misra, P. Das, N. Singh, *J. Lumin.* **2014**, *154*, 502–510; b) O. Stern, M. Volmer, *Physik. Z.* **1919**, *20*, 183–188.

[33] H. M. Irving, R. J. P. Williams, *J. Chem. Soc.* **1953**, 3192–3210.

[34] A. J. Bard, L. R. Faulkner, *Electrochemical Methods: Fundamentals and Applications*, 2nd ed., John Wiley & Sons, **2000**.

[35] a) J. J. Colleran, B. S. Creaven, D. F. Donlon, J. McGinley, *Dalton Trans.* **2010**, *39*, 10928–10936; b) S. Meddeb-Limem, S. Besbes-Hentati, H. Said, M. Bouvet, *Electrochim. Acta* **2011**, *58*, 372–382; c) A. Louati, J. Spraula, V. Gabelica, P. Kuhn, D. Matt, *Electrochem. Commun.* **2006**, *8*, 761–766; d) A. Pailleret, G. Herzog, D. W. M. Arrigan, *Electrochem. Commun.* **2003**, *5*, 68–72.

[36] J. K. H. Wong, M. H. Todd, P. J. Rutledge, *Molecules* **2017**, *22*, 200–228.

[37] R. C. Knighton, P. D. Beer, *Chem. Commun.* **2014**, *50*, 1540–1542.

[38] R. Lavendomme, L. Troian-Gautier, S. Zahim, O. Reinaud, I. Jabin, *Eur. J. Org. Chem.* **2016**, *2016*, 1665–1668.

[39] G. Singh, S. Rani, A. Saroa, S. Girdhar, J. Singh, A. Arora, D. Aulakh, M. Wriedt, *RSC Adv.* **2015**, *5*, 65963–65974.

[40] C. D. Geary, S. G. Weber, *Anal. Chem.* **2003**, *75*, 6560–6565.

[41] J.-S. Lee, J. W. Lee, Y.-T. Chang, *J. Comb. Chem.* **2007**, *9*, 926–928.

[42] S. Sun, W. Hu, H. Gao, H. Qi, L. Ding, *Spectrochim. Acta Part A* **2017**, *184*, 30–37.